doi:10.1016/j.jmb.2012.04.006 J. Mol. Biol. (2012) 420, 112–127

Contents lists available at www.sciencedirect.com

Journal of Molecular Biology

journal homepage: http://ees.elsevier.com.jmb

The β-Scaffold of the LOV Domain of the *Brucella* Light-Activated Histidine Kinase Is a Key Element for Signal Transduction

Jimena Rinaldi [1]†, Mariana Gallo [1]†, Sebastián Klinke [1], Gastón Paris [1], Hernán R. Bonomi [1], Roberto A. Bogomolni [2], Daniel O. Cicero [1] and Fernando A. Goldbaum [1]*

[1]*Fundación Instituto Leloir, IIBBA-CONICET, Ciudad Autónoma de Buenos Aires, C1405BWE, Argentina*
[2]*Department of Chemistry and Biochemistry, University of California, Santa Cruz, CA 95064, USA*

Received 18 January 2012; received in revised form 4 April 2012; accepted 5 April 2012
Available online 11 April 2012

Edited by C. Kalodimos

Keywords:
LOV domain; histidine kinase; *Brucella*; X-ray crystallography; NMR spectroscopy

Light–oxygen–voltage (LOV) domains are blue-light-activated signaling modules present in a wide range of sensory proteins. Among them, the histidine kinases are the largest group in prokaryotes (LOV-HK). Light modulates the virulence of the pathogenic bacteria *Brucella abortus* through LOV-HK. One of the striking characteristic of *Brucella* LOV-HK is the fact that the protein remains activated upon light sensing, without recovering the basal state in the darkness. In contrast, the light state of the isolated LOV domain slowly returns to the dark state. To gain insight into the light activation mechanism, we have characterized by X-ray crystallography and solution NMR spectroscopy the structure of the LOV domain of LOV-HK in the dark state and explored its light-induced conformational changes. The LOV domain adopts the α/β PAS (PER-ARNT-SIM) domain fold and binds the FMN cofactor within a conserved pocket. The domain dimerizes through the hydrophobic β-scaffold in an antiparallel way. Our results point to the β-scaffold as a key element in the light activation, validating a conserved structural basis for light-to-signal propagation in LOV proteins.

Introduction

Proteins that sense environmental signals play a crucial function for cellular adaptation in response to changing conditions. LOV (light, oxygen, and voltage) domains, first discovered in plants, are well-characterized sensory modules of ca 100 residues building up quite compact α/β structures. They are defined as a subset of the larger PER-ARNT-SIM (PAS) domain superfamily[1] that specifically binds a flavin cofactor (either FMN or FAD), which confers blue-light-sensing function. The LOV domain core has a classical PAS fold, consisting of a five-stranded antiparallel β-sheet (Aβ, Bβ, Gβ, Hβ, and Iβ) and helical connector elements (Cα, Dα, Eα, and Fα). LOV domains are distributed in all *three kingdoms of life* with the only exception of animals. They are found in regulatory proteins involved in phototropism,[2] seasonal gene transcription,[3] and bacterial stress responses,[4] among others, controlling a wide range of effector domains. It is not yet understood how these light-regulated domains with similar tertiary structures control such a wide variety of effectors.

*Corresponding author. E-mail address: fgoldbaum@leloir.org.ar.

† J.R. and M.G. contributed equally to this work.

Abbreviations used: LOV, light–oxygen–voltage; LOV-HK, LOV histidine kinase; PAS, PER-ARNT-SIM; AsLOV2, *Avena sativa* Phototropin1 LOV2 domain; HT, head-to-tail; HH, head-to-head; PDB, Protein Data Bank; HSQC, heteronuclear single quantum coherence; NOE, nuclear Overhauser enhancement; EDTA, ethylenediaminetetraacetic acid.

Upon illumination, LOV domains form a covalent adduct between the S^{γ} atom on a conserved cysteine residue and the C4(a) atom of the flavin molecule.[5,6] This event generates structural changes that propagate to the domain surface, altering the interactions of the LOV domain core with intra- or interprotein partners. For example, structural studies on *Avena sativa* Phototropin1 LOV2 domain (AsLOV2) demonstrated light-induced unfolding of the Jα-helix located C-terminal to the canonical LOV domain.[7] Similarly, the *Neurospora crassa* VIVID protein reorients an N-terminal extension of its LOV domain upon illumination.[8] In the light-regulated DNA-binding protein EL222, light disrupts the interaction between the LOV domain and the DNA-binding domain.[9] The LOV domains of the dimeric YtvA protein from *Bacillus subtilis* form a surface for dimerization.[10,11] A light-induced small structural rearrangement is proposed to drive a scissor-like rotation of the two monomers relative to each other.[11] In all cases, the protein partners interact with the β-sheet surface of the LOV domain, suggesting a common site for signal propagation. The functional importance of light-regulated interactions at this site has been validated by the fact that point mutations on the β-sheet or interacting effector surfaces decouple protein activity from adduct formation.[8,12–16]

LOV domains show, to a different degree, a tendency to dimerize, with or without the assistance or competition of the helical flanking regions.[17] Besides conveying signal propagation, the β-scaffold is also involved in LOV–LOV dimerization. *In vitro* isolated LOV domains adopt an antiparallel head-to-tail (HT)[18–20] or a parallel head-to-head (HH)[10,11,21] arrangement.

The photochemistry of a number of prokaryotic and eukaryotic LOV domains has been characterized *in vitro*. The rate at which the adduct species decay to the ground state (i.e., kinetics of cysteinyl-flavin adduct rupture) ranges over 5 orders of magnitude from seconds to hours.[16] Some differences in the kinetics of adduct formation and rupture among LOV domains can be explained by variation in the residues that build up the binding pocket of the flavin cofactor. However, in other cases, the adduct lifetime is modulated by non-conserved regions of structure outside the defined LOV domain core.[16]

Bacterial genomes present LOV domains coupled to a variety of signaling output domains.[22–26] Among this diverse set, the largest group, approximately 50% of bacterial LOV proteins, corresponds to the LOV histidine kinases (LOV-HKs).[27]

Brucella spp. are facultative intracellular animal pathogens that encode an invariable LOV-HK protein in all genomes sequenced to date. *Brucella* LOV-HK exhibits an increase in histidine autophosphorylation upon absorption of blue light. Exposure of wild-type *B. abortus* to visible light results in a 10-fold higher level of bacterial replication in mouse macrophages than the corresponding dark control.[28] This light-dependent virulence enhancement is mediated by LOV-HK.

The aim of the present work is to describe the blue-light-sensing mechanism of LOV-HK from *B. abortus*. By means of X-ray crystallography and solution NMR spectroscopy, we have characterized the structure of the LOV domain of LOV-HK in the dark state and explored its light-induced conformational changes. Our results point to the β-scaffold as a key element in the light-to-signal propagation.

Results

Identification and photochemical activity of a stable fragment of the sensory domain of LOV-HK from *B. abortus*

LOV-HK from *B. abortus* is formed by a LOV domain core at the N-terminus followed by PAS and histidine kinase domains at the C-terminus. It does not present transmembrane regions, which suggests that LOV-HK is located in the cytoplasm of the bacteria. LOV and PAS domains are connected by a linker region, which is predicted to bear a so-called Jα-helix moiety as in AsLOV2, YtvA, and EL222 LOV domains (Fig. 1a). According to secondary-structure predictions, *Brucella* LOV-HK Jα-helix is estimated to be 34 residues long (residues 135–168) with no sequence similarity to other known LOV proteins (Fig. 1a). Additionally, this region presents a coiled-coil signature based on the Lupas/Stock[29] algorithm and the Paircoil algorithm of Berger and Keating,[30] as observed for LOV-HK from *Caulobacter crescentus*,[16] Ytva LOV domain, and many PAS-HKs.[31]

As an initial step to elucidate the molecular mechanism of light activation of LOV-HK from *B. abortus*, we aimed to determine the crystal structure of the light receptor LOV domain. First, a construct comprising both the LOV core and the subsequent 20 Jα-helix residues (LOVcore+$J\alpha_{20}$) was chosen for crystallization. The extent of the Jα-helix included in this construct was decided on the basis of the crystallization of AsLOV2.[32] After several trials, no crystals were obtained. Spontaneous proteolysis of the LOVcore+$J\alpha_{20}$ construct was observed in the crystallization drops as well as in the protein preparation stored at 4 °C. Taking into account the susceptibility to proteolysis of this construct, we searched for a more stable fragment by limited proteolysis with papain. The proteolytic products were analyzed by mass spectrometry and N-terminal sequencing (Fig. 1b). As a result, two fragments lacking the last 15 and 22 C-terminal residues from the original construct were identified. The latter was discarded as the truncation takes place on the last β-strand of the conserved PAS fold of the LOV domain. On the other hand, the former construct

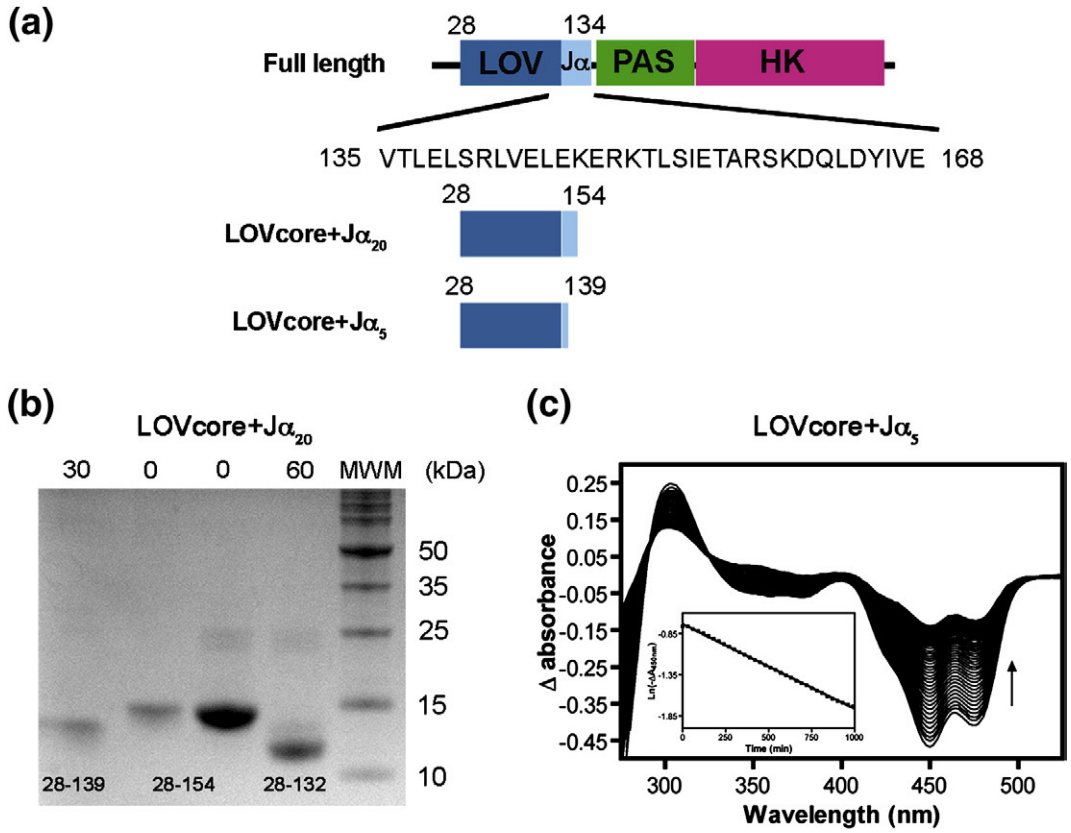

Fig. 1. Identification of a stable fragment of LOV-HK LOV domain from *B. abortus* and its photochemical activity. (a) Domain organization of LOV-HK and the working constructs. The sequence of the Jα-helix predicted by secondary-structure analysis is shown. (b) Limited proteolysis with papain of the LOVcore+$J\alpha_{20}$ construct (28–154) reveals two bands corresponding to the C-terminal truncations 28–139 and 28–132 (indicated at the bottom of the gel). The central lanes correspond to two different protein quantities at the starting point of the incubation. The side lanes correspond to 30 min and 60 min of incubation as indicated. (c) Light-induced difference absorption spectra of the LOVcore+$J\alpha_5$ construct. Data were collected every 30 min after light excitation. The arrow indicates the temporal evolution. The insets show the temporal evolution of the absorption changes at 450 nm. The LOVcore+$J\alpha_5$ construct does recover very slowly to the dark state after illumination (half-life: 573 min at 20 °C and pH 6.5).

contains all the predicted PAS secondary structural elements and thus was chosen for crystallization. This construct, which we called LOVcore+$J\alpha_5$, comprises the residues 28–139 from the full LOV-HK protein, including the first five residues from the Jα-helix. Taking into account the presence of an N-terminal three-residue cloning artifact (MAS) and a C-terminal thrombin cleavage site followed by a 6× His-tag (LVPRGSLEHHHHHH), the polypeptide chain comprises a total of 128 residues (Fig. S3a). Due to the inefficiency of the thrombin cleavage, we skipped this step in the purification.

We noticed that the LOVcore+$J\alpha_5$ construct returns to the dark state upon illumination, as the illuminated colorless sample recovers its yellow appearance after storage at 4 °C. For this reason, we decided to study the photochemical behavior of the LOVcore+$J\alpha_5$ construct (Fig. 1a) through UV–Vis absorption[28] and NMR spectroscopy (see Fig. S1 and Materials and Methods).

The adduct state of the full-length LOV-HK protein is extremely stable and does not decay measurably in hours.[28] In contrast, the LOVcore+$J\alpha_5$ construct shows a first-order exponential dark-state recovery (Fig. 1c and Fig. S1d), with a half-life of 573 min at 20 °C and pH 6.5. This result demonstrates that regions of the protein beyond the boundaries of this construct lock the photocycle.

As previously observed for other LOV domains,[6,33] there is a marked pH dependence of the dark recovery rate. Half-lives of 350 and 105 min are observed at pH 7.0 and 8.0 at 35 °C, respectively, which is consistent with a base-catalyzed process (Fig. S1d). To gain insight into the thermodynamics of the regeneration of the dark state, we carried out an Arrhenius analysis of the temperature dependence of the lit state lifetime (Fig. S1e). The E_{act} thus obtained is 125.9 ± 4.9 kJ/mol and the pre-exponential factor is 7×10^{16} s^{-1}.

Table 1. X-ray data collection and refinement statistics

Data collection	
Number of frames	250
Wavelength (Å)	1.542
Indexing and scaling	
Cell parameters (Å)	
a	37.90
b	61.60
c	98.60
Space group	$P2_12_12_1$
Resolution limit (Å)	1.64
Number of unique reflections	28,520
Multiplicity	4.6 (4.3)[a]
I/σ	22.7 (4.4)
R_{merge} (%)	3.7 (28.5)
Completeness (%)	98.5 (94.6)
Number of molecules per asymmetric unit	2
Solvent content (%)	38.4
B-factor (Wilson plot; Å^2)	26.2
Refinement	
Resolution limits (Å)	20.0–1.64
R-factor	0.195
R_{free}	0.222
Non-hydrogen protein atoms	1726
Non-hydrogen ligand atoms	62
Solvent molecules	159
r.m.s.d. bond lengths (Å)	0.016
r.m.s.d. bond angles (°)	1.574
Average *B*-factor (Å^2)	20.8
Ramachandran plot	
Most favored (%)	93.7
Additional allowed (%)	6.3
Generously allowed (%)	—
Disallowed (%)	—

[a] Values in parentheses correspond to the highest-resolution shell (1.64–1.68 Å).

The fact that we were able to generate a stable LOV domain fragment, and that this fragment spontaneously decays to the dark state, allowed us to structurally characterize the dark state of the LOV sensory domain, as described below.

Structural characterization of the LOV domain in the dark state

Crystal structure of the LOV domain in the dark state

The LOVcore+Jα_5 construct (residues 28–139 plus N- and C-terminal cloning artifacts, giving a total of 128 residues) was crystallized, and its structure was solved in the dark conformation at 1.64 Å resolution by the molecular replacement method using AsLOV2 [Protein Data Bank (PDB) code 2V0U] as search model. The final structure was refined to $R = 0.195$ and $R_{free} = 0.222$ and shows very good geometric parameters, with more than 93% of the residues lying in the most favorable region of the Ramachandran plot. A total of two molecules, designated as A and B, were found in the asymmetric unit. Both main chains present continuous density in the $2F_o - F_c$ Fourier map with no breaks. However, the first residue as well as the last 12 lack electron density for chain A, as the first 5 and last 15 do for chain B. Most of the missing residues correspond to the N- and C-terminal cloning artifacts. The electron density observed includes residues 28 to 139 from chain A and residues 30 to 137 from chain B (chain A: Ala-Ser-28→139-Val; chain B: 30→137). Additionally, five polar residues that are exposed to the solvent, namely, Lys93 and Arg124 from both chains and Asn122 from chain B, show no electron density for their side chains and were modeled as alanine. Each polypeptide chain also binds an FMN molecule that is clearly defined in the Fourier map. To finish, we added a total of 159 water molecules to the model in the last stages of the refinement process. Both copies in the asymmetric unit are essentially equivalent, with a C^α root-mean-square deviation (rmsd) of 0.43 Å for 107 superimposed residues. Data collection and refinement statistics are summarized in Table 1.

The LOV domain adopts the expected α/β PAS domain fold, with four α-helices (C, D, E, and F) and five β-strands (A, B, G, I, and H) (Fig. 2a and d). A single FMN molecule is buried within a conserved pocket (Fig. S2). The domain has a β-sheet face, which is mainly hydrophobic, and a charged α-helical face. The *Brucella* LOV structure is very similar to other LOV domains, with the main structural differences located at the H–I loop (Fig. 2d).

There are three main conformational features concerning the lit and the dark states, which are present in all LOV domains known to date:[11,17,27,32] (1) The presence of more than one rotamer of the side chain of the reactive cysteine residue, with its S^γ atom approximately 3 Å apart from the FMN

Fig. 2. The crystal structure of LOV-HK LOV domain from *B. abortus* in the dark state adopts the typical α/β PAS domain fold and shows conserved conformational features. (a) Overall structure. The secondary structural elements are indicated. (b) The electron density map of the FMN molecule shows that the ligand is planar and reveals the lack of electron density between Cys69 and the flavin ring. The S^γ atoms of both Cys69 conformers are 3 Å away or more from the C4(a) atom of the FMN molecule. The $2F_o - F_c$ density map is contoured at 2 σ. (c) The amide nitrogen atom of Gln132 of the Iβ-strand points to the O4 atom of the FMN ligand. (d) Structure-based sequence alignment of LOV domains: Phototropin1 LOV2 domain from *A. sativa* (LOV2_Phot1_Asa), Phototropin LOV1 domain from *Chlamydomonas reinhardtii* (LOV1_Phot_Cre), YtvA LOV domain from *B. subtilis* (YtvA_Bsu), EL222 LOV domain from *Erythrobacter litoralis* (EL222_Eli), Phototropin2 LOV1 domain from *Arabidopsis thaliana* (LOV1_Phot2_Ath), and Vivid LOV domain from *N. crassa*. The color coding is the same as in (a). The identity percentage and the rmsd values of the complete LOV domain (rmsd) and of the LOV domain excluding the H–I loop (rmsd w/o H–I loop) compared to the LOV-HK LOV domain from *B. abortus* are indicated in the right margin of each sequence.

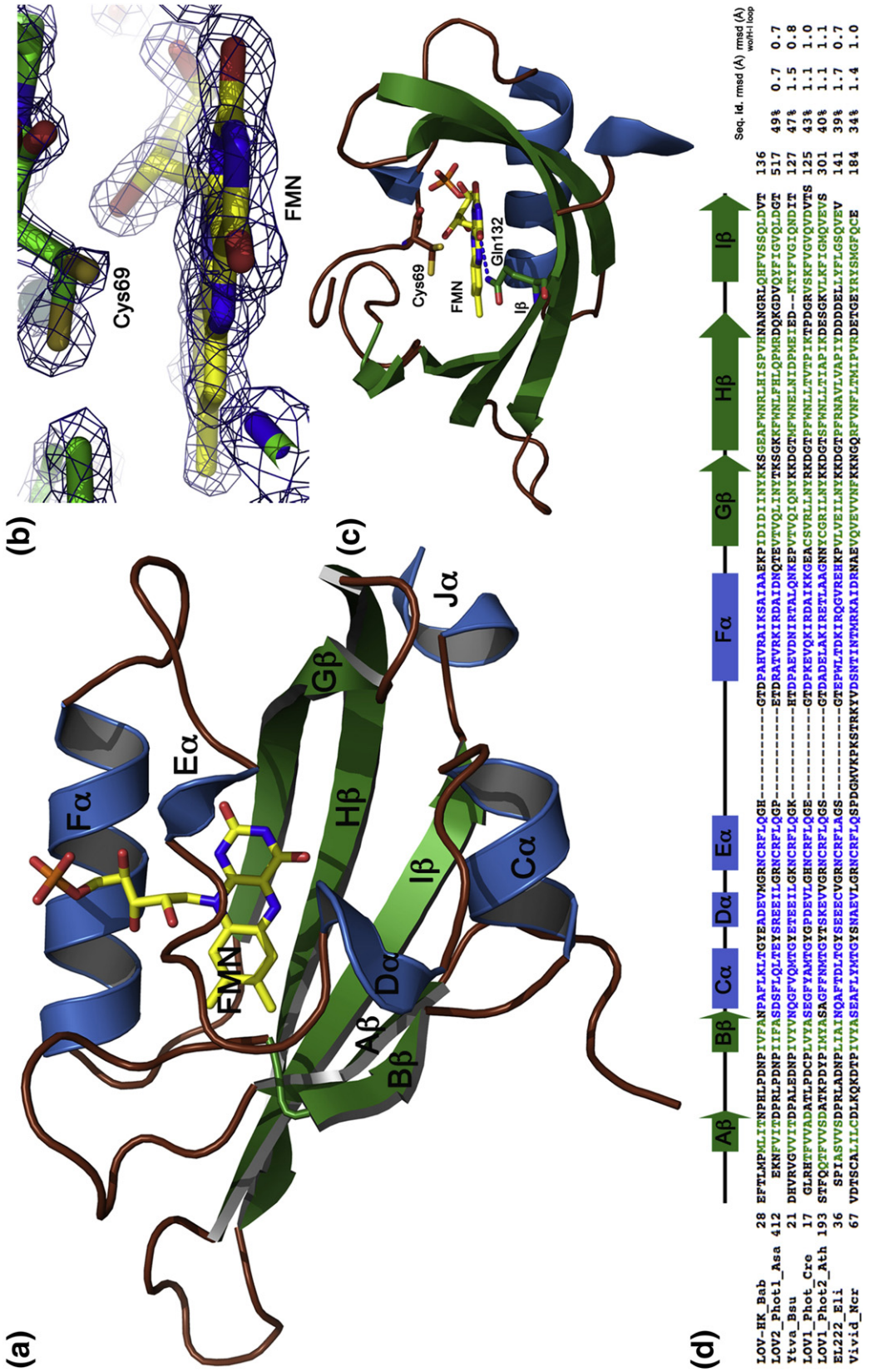

Fig. 2 (*legend on previous page*)

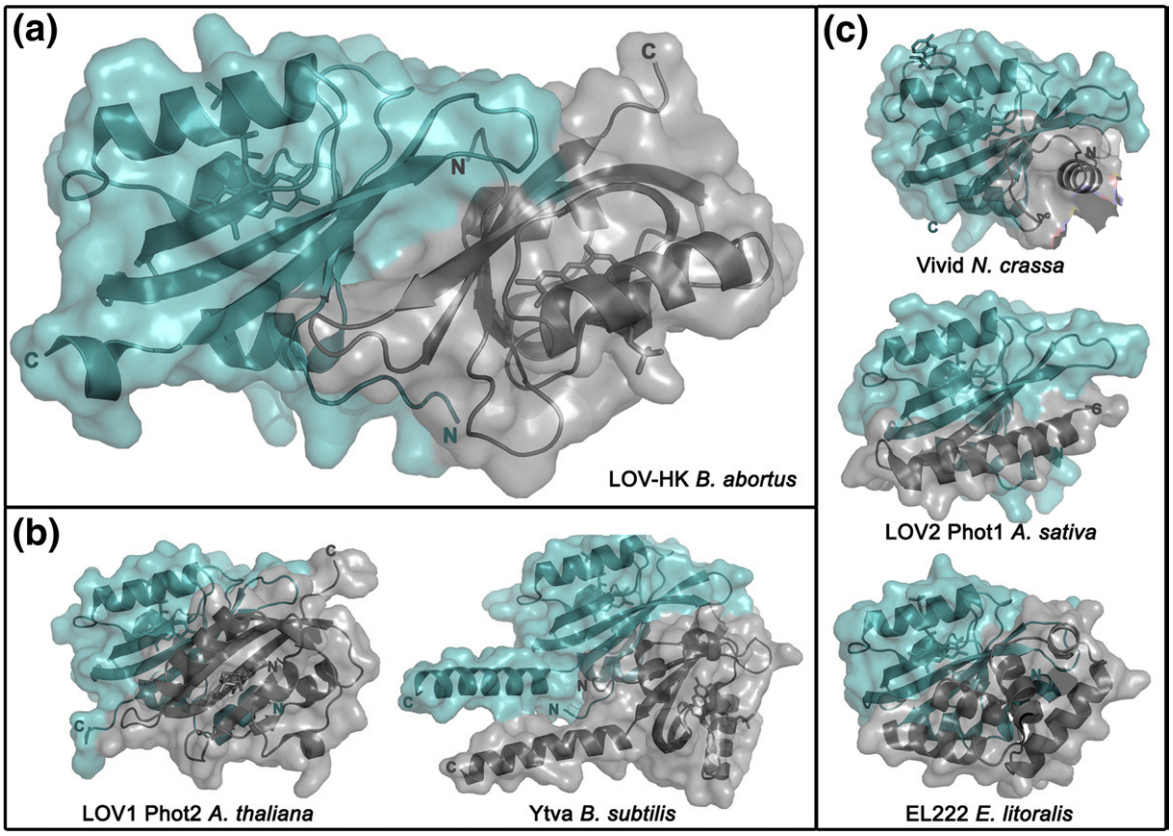

Fig. 3. The β-scaffold is buried in all LOV domain structures. (a) Crystallographic HT dimer of the *Brucella* LOV domain. (b) Other crystallographic dimers in which the β-sheet is involved in the dimerization: Phototropin2 LOV1 domain HT dimer from *A. thaliana* and YtvA LOV domain HH dimer from *B. subtilis*. (c) Crystallographic LOV domains in which the β-sheet is involved in intramolecular interactions: Vivid LOV domain from *N. crassa*, Phototropin1 LOV2 domain from *A. sativa*, and EL222 from *E. litoralis*. N- and C-termini are indicated.

molecule in the dark conformation. In the lit state, there is only one conformer at about 2 Å from the C4(a) atom of the FMN molecule. (2) The planarity of the FMN isoalloxazine ring. In the dark state, the FMN molecule is planar, whereas in the lit state, the planarity is broken by the C4(a) atom, which becomes an sp^3-hybridized carbon upon binding to the reactive cysteine residue. (3) The side chain of a conserved FMN-interacting glutamine residue in the Iβ-strand. In the dark state, its terminal amide nitrogen atom is hydrogen bonded to the O4 atom of the FMN molecule, while in the lit state, its side chain is rotated by 180°, with its carbonyl group pointing to the N5 atom of the FMN molecule. These features are conserved in the *Brucella* LOV domain in its dark state. The reactive Cys69 residue presents two rotamers, with its S^{γ} atom apart from the FMN molecule (Fig. 2b). The isoalloxazine ring of the FMN molecule is planar (Fig. 2b). Finally, the side chain of Gln132 forms a hydrogen bond to the O4 atom of the FMN molecule (Fig. 2c).

Within the asymmetric unit of the crystal, two molecules of the LOV domain related by a dyad axis form an HT antiparallel dimer (Fig. 3a). The dimerization interface involves most of the β-sheet (strands A, B, H, and I). It buries 880 $Å^2$ (13.6%) of solvent-accessible surface area. The contacts between both monomers are mostly hydrophobic (70% of the interfacing area). The Complexation Significance Score from the European Molecular Biology Laboratory, European Bioinformatics Institute, Protein Interfaces, Surfaces and Assemblies server‡ yields a value of 0.492 for the crystal structure. This value implies that the existence and/or the stability of the dimer in solution are ambiguous and that the actual oligomeric state should be confirmed by solution approaches. The antiparallel orientation of the LOV domain dimer in the crystal structure might not be the one adopted by both LOV domains in the complete dimeric protein (see Discussion).

As mentioned before, the LOVcore+$J\alpha_5$ construct bears the first five residues of the connecting Jα-helix (VTLEL). All these residues are clearly seen in the electron density in chain A, whereas only the first three are present in chain B. As predicted, these

‡ www.ebi.ac.uk

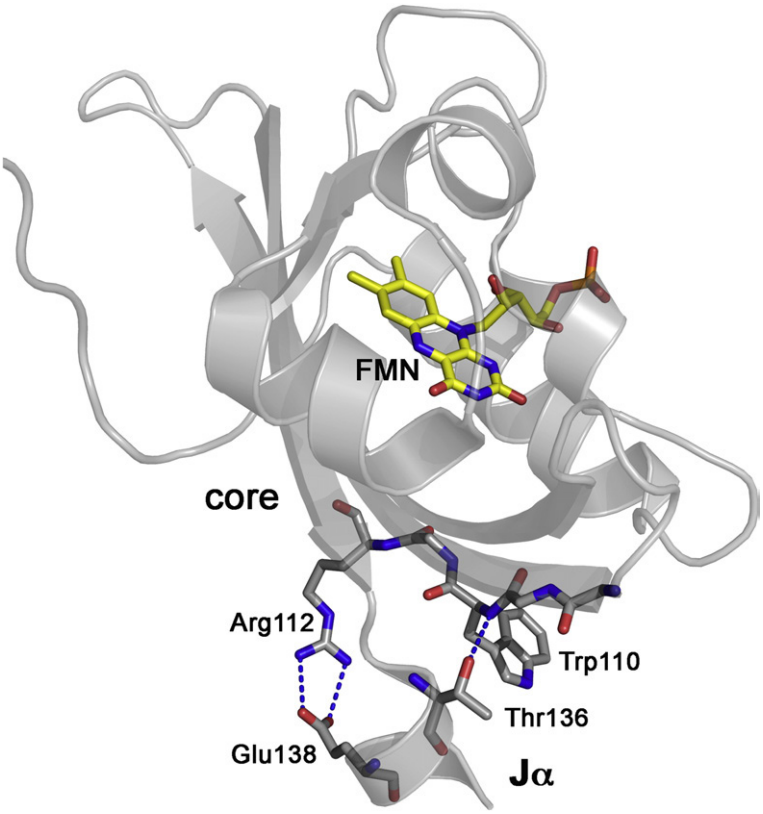

Fig. 4. The Jα-helix points towards the solvent. Two polar interactions account for its orientation: a salt bridge between Arg112 and Glu138, and a hydrogen bond between Trp110 and Thr136. The main chain is shown as a cartoon, and the side chains of the contacting residues as well as the backbone from residues 109–112 are shown as sticks.

residues adopt a helical conformation. In both monomers, the Iβ-strand is directly followed by the Jα-helix with no loop in between (Fig. 4). The Jα-helix points towards the solvent, having the same orientation in both monomers. Two polar interactions that involve residues from the β-scaffold are key for the Jα-helix orientation: a salt bridge between Arg112 and Glu138, and a hydrogen bond between the Trp110 amide and Thr136 hydroxyl groups.

Solution conformation of the LOV domain in the dark state

We applied NMR spectroscopy to study the conformation of the LOVcore+$J\alpha_5$ construct both in its dark and lit states in solution. This enabled us to investigate the light-driven changes in the protein. We first analyzed the dark state. By using standard 2D and 3D experiments, we assigned 82 out of 104 (79%) backbone nuclei of the LOV domain (Fig. 5a). We accounted for almost all cross peaks present in the $^{15}N–^{1}H$ heteronuclear single quantum coherence (HSQC) spectrum. Those that could not be assigned did not present correlations in the 3D spectra of the protein. With the exception of His75, which is probably lost due to solvent exchange as it belongs to an exposed loop, all missing residues are part of the β-scaffold that is involved in the dimerization interface in the crystal structure (Fig. 5b). Some of these residues possibly undergo conformational exchange that broadens the peaks beyond detection. The interface missing cross peaks did not appear in the $^{15}N–^{1}H$ HSQC spectra after a 10-fold dilution.

TALOS+ analysis[34] of the backbone nuclei chemical shifts shows that the secondary structure of the LOV domain in solution is in very good agreement with that of the crystal (Fig. S3). Interestingly, residues corresponding to the N-terminal region of the Jα-helix, which are included in the LOVcore+$J\alpha_5$ construct, also adopt a helical conformation in solution as observed in the crystal structure. Furthermore, long-range $^{1}H–^{1}H$ nuclear Overhauser enhancements (NOEs) were detected in the ^{15}N-edited NOESY (nuclear Overhauser enhancement spectroscopy) spectrum between Trp110 and Thr136, supporting the presence in solution of the hydrogen bond between the Trp110 amide and Thr136 hydroxyl groups, as observed in the crystal (Fig. 4). This interaction may contribute to the orientation of the helix with respect to the core.

^{15}N relaxation data were measured for the LOV domain in the dark state (Fig. S4). Residues near the unassigned region, which correspond to the interface (see Fig. 5b), present relatively reduced T_2 values. This is indicative of slow conformational motions (microsecond-to-millisecond timescale) that broaden the signals and suggests that this region suffers some kind of conformational instability. On

the other hand, the ^{15}N relaxation data indicate that the rest of the protein including the Jα-helix fragment is well structured, with little evidence of fast internal motions, as shown by the ^{15}N–^{1}H NOE that presents a rather uniform behavior, with a mean value of 0.82 (Fig. S4). The only flexible region is the C-terminal end, with low T_1 and high T_2 values and with small or negative NOEs. This region

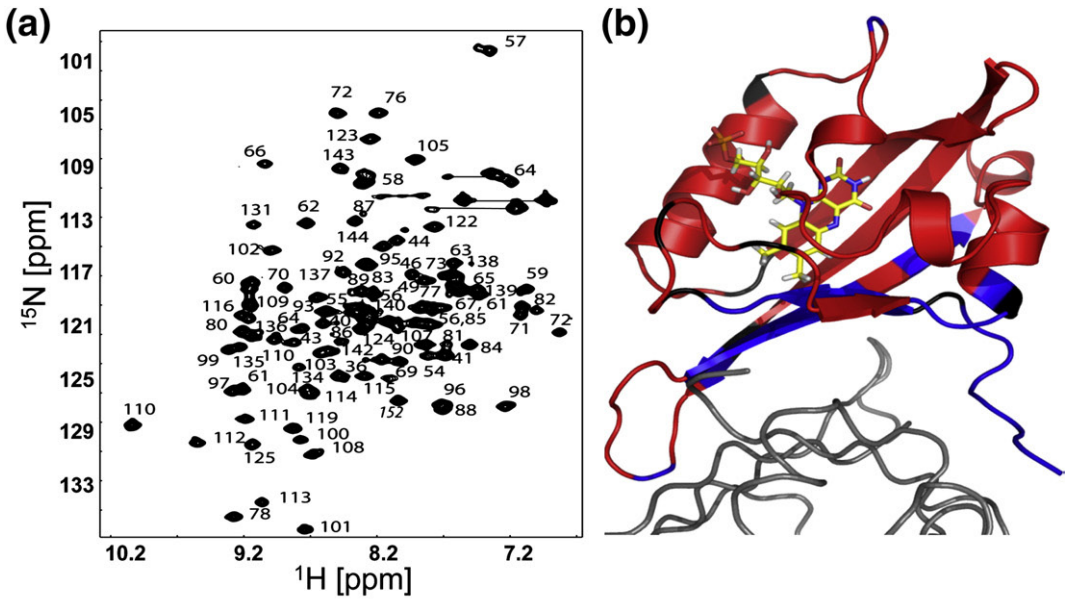

(c)

Object	R_h [Å]	D_x:D_y:D_z
Monomer	19	1.0 : 1.1 : 1.3
HT	25	1.0 : 1.0 : 1.6
HH	24	1.1 : 1.0 : 1.3
Experimental	24.2 ± 0.4	-

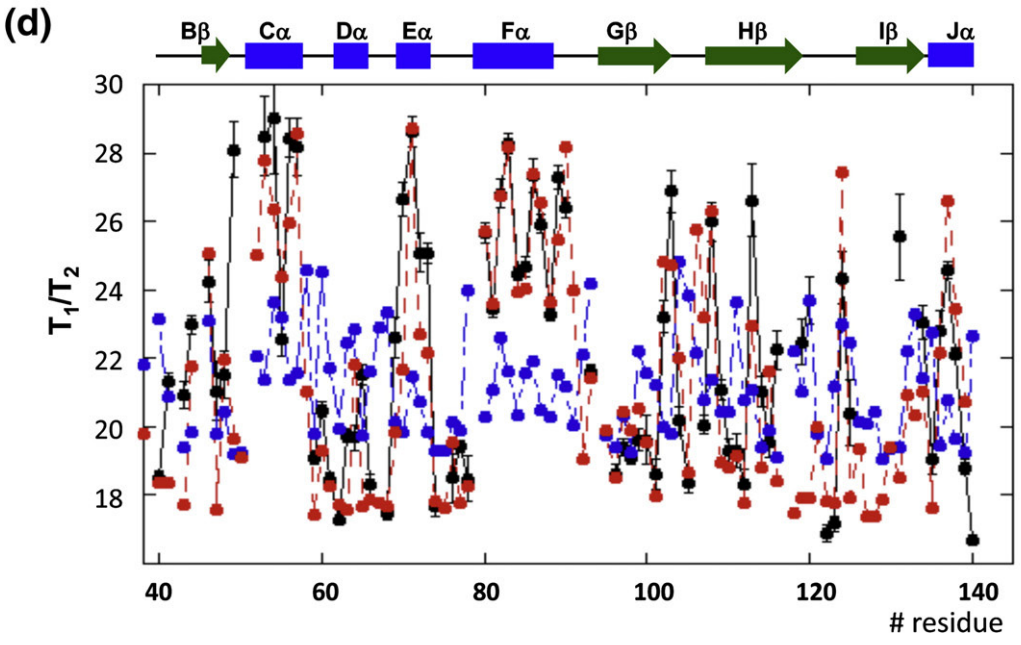

Fig. 5 (*legend on next page*)

involves residues 143–145, belonging to the C-terminal cloning artifact.

The rotational correlation time obtained from the ^{15}N relaxation data is 14.5 ns. This value is consistent with the presence of a dimer in solution. In order to analyze the oligomeric state and, consequently, the quaternary structure of the LOV domain in solution, we performed diffusion measurements in dark conditions. The hydrodynamic radius (R_h), determined using dioxane as internal standard,[35] was 24.2 ± 0.4 Å (Fig. 5c). Furthermore, the R_h did not vary over the protein concentration range from 0.06 to 1 mM (data not shown), ruling out significant aggregation phenomena of the LOV domain in the experimental conditions. The calculated R_h for the crystallographic monomer using the program HYDRONMR[36] is 19 Å, while for the crystallographic HT dimer and an artificial HH dimer, the calculated R_h values are 24 and 25 Å, respectively. Therefore, the experimental R_h is consistent with the presence in solution of an HT or an HH dimer. Additionally, the equilibrium dissociation constant of the dimer (K_d) should be much smaller than 0.06 mM, which explains the fact that the interface missing cross peaks did not appear in the ^{15}N–^{1}H HSQC spectra after diluting the sample up to 0.08 mM.

Since the signals corresponding to residues of the β-sheet face that form the dimerization interface do not appear in the NMR spectra, examination of NOE interactions between protons belonging to the interface cannot be used to discriminate between the two possible dimers. Consequently, an alternative approach based on the dependence on rotational diffusion anisotropy of ^{15}N relaxation measurements was used. Variations in T_1/T_2 ratio values can be due to internal motions or to the anisotropic rotational diffusion of the molecule. In nonspherical molecules, the ^{15}N relaxation parameters T_1 and T_2 depend on the orientation of the ^{15}N–^{1}H bond relative to the unique axis of the diffusion tensor. Therefore, the T_1/T_2 ratios give structural information at the molecular level for each NH bond vector.[37]

Figure 5d shows the experimental and the calculated T_1/T_2 values for the HH and HT dimers using the HYDRONMR software, plotted against the peptidic sequence. The calculated T_1/T_2 ratios for the HT dimer but not for the HH dimer nicely reproduce the experimental T_1/T_2 profile at the residue level. The rmsd values between calculated and experimental values of these ratios are 2.3 and 4 for the HT and HH dimers, respectively. In addition, if residues probably involved in slow conformational motions, with significantly short T_2 values (Fig. S6), are excluded, the rmsd for the HT dimer decreases from 2.3 to 1.7. These results strongly support that the LOV domain exists in solution as the HT crystallographic dimer.

Light-induced conformational changes in the LOV domain

Several unsuccessful attempts to obtain the crystal structure of the lit state of the LOV domain have been made. No crystal grew under blue light illumination. Irradiated crystals grown in the dark showed an increased mosaicity with an important proportion of the data corresponding to the dark-state structure, revealing that the crystal packing locks the molecules in the dark conformation. Thus, we decided to apply NMR spectroscopy to study the conformational changes triggered by light exposure. Upon illumination, several chemical shift and peak intensity changes in the ^{15}N–^{1}H HSQC (Fig. 6a) and ^{13}C–^{1}H HSQC spectra (Fig. S5) were observed. Changes in chemical shifts reflect alterations in the local electronic environment around nuclei, while line broadening is symptomatic of dynamic behavior on the microsecond-to-millisecond timescale and/or different solvent exchange contributions. The chemical shift dispersions in the dark and lit conditions are similar, indicating that there is no domain unfolding induced by light, as observed in AsLOV2.[7] However, we noticed that the LOV domain in the lit state is more susceptible to proteolysis than in the dark state. After 5 days under illumination, the protein shows evidences of degradation, both by SDS-PAGE and in NMR spectra, which are not observed in darkness. Nevertheless, we were able to assign 75 out of 104 (72%) amide nuclei of the protein in the lit state. TALOS+ analysis of the backbone chemical shifts shows that the secondary-structure elements are the same as in the dark state (Fig. S3).

To identify the regions of the molecule that experience light-dependent changes and to quantify

Fig. 5. In solution, the LOV domain in the dark state is an HT dimer, with a conformationally unstable dimerization interface comprising the β-scaffold. (a) ^{1}H–^{15}N HSQC spectrum of the LOVcore+Jα$_5$ construct in the dark state. (b) The backbone chemical shift assignment is mapped on the crystallographic structure. The FMN molecule is depicted in yellow, the assigned residues are in red, the missing residues are in blue, and the prolines are in black. The second monomer is shown in gray. (c) Experimental and calculated hydrodynamic radii for the LOV monomer and for the HH and HT dimers. The components of the rotational diffusion tensor (D_x, D_y, D_z) are also reported for the three molecules. (d) T_1/T_2 ratio per residue. Experimental (black circles) and calculated T_1/T_2 values for the HT (red circles) and for the HH (blue circles) dimers are plotted as a function of the residue number. Secondary-structure elements are indicated in the upper part. The unassigned N-terminal region (Met-Ala-Ser-28 → 40) and the C-terminal residues corresponding to the thrombin cleavage site and the His-tag, which are absent in the coordinate file, were not included in the plot.

those changes, we analyzed the chemical shift perturbations (Fig. 6b) and mapped them onto the crystal structure (Fig. 6c). In particular, residues belonging to the N-terminal end of the Jα-helix do not modify their chemical shifts upon illumination. On the other hand, the largest differences were observed in the αE-helix, which contains the active cysteine, and in the Hβ- and Iβ-strands. Also, the

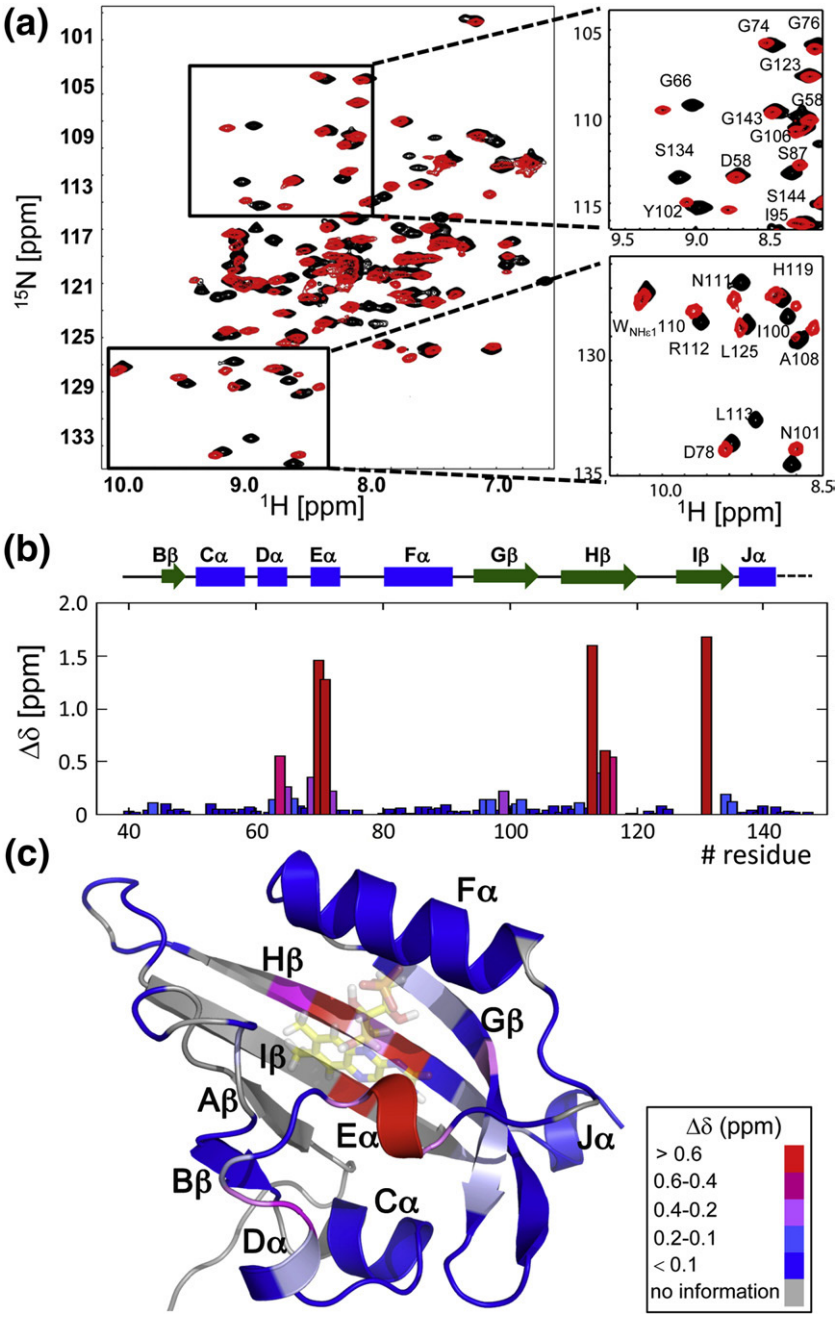

Fig. 6. Light-induced conformational changes. (a) Superposition of the ^{1}H–^{15}N HSQC spectra of the LOV domain in the dark and lit states (black and red, respectively). The insets show selected regions of the spectra in which the chemical shift assignment is indicated. (b) Chemical shift perturbation analysis. Δδ corresponds to $\Delta\delta_{av}=[(\Delta\delta^2_{NH}+\Delta\delta^2_{N}/25)/2]^{1/2}$ [38] for positions assigned both in the lit and dark states, while $\Delta\delta_{min}=[(\Delta\delta^2_{NH}+0.17*\Delta\delta^2_{N}+0.39*\Delta\delta^2_{CO})]^{1/2}$ [39] for residues assigned only in the dark state (i.e., Cys69, Arg70, Phe71, Leu113, His114, Ile115, and Ser116). Regions of secondary structure are shown in the upper part of the figure. The unassigned N-terminal region (Met-Ala-Ser-28→40) is not included in the plot. The residues corresponding to the C-terminal cloning artifact are represented with a broken line. (c) Values from (b) are mapped on the dark-state crystal structure with a color gradient encoding the magnitude of the shift change.

Gβ-strand and the αD-helix, which are not in the immediate surroundings of the FMN molecule, exhibit significant perturbations.

Taken together, the LOV domain suffers a light-induced destabilization without global unfolding. The light-triggered conformational changes are concentrated in the β-scaffold, pointing it as a key transducer element for signal propagation to the effector domain.

Discussion

We have shown that light modulates the virulence of the pathogenic bacteria *B. abortus* through LOV-HK.[28] This protein has the capacity to autophosphorylate upon absorbing blue light photons. The signal is then transferred to PhyR, a response regulator that modulates the expression of several genes using the General Stress Response (unpublished results). One of the striking characteristics of LOV-HK is the fact that the protein remains activated upon light sensing, without recovering the basal state in the darkness (truncated photocycle). Here, we analyzed the structure and the signal transduction mechanisms of the LOV domain of the *Brucella* virulence factor LOV-HK, describing for the first time the three-dimensional characteristics of a bacterial LOV domain linked to a histidine kinase. Our analysis using X-ray crystallography combined with NMR spectroscopy in light and dark conditions allowed us to understand the roles of the β-scaffold in the signal propagation and the quaternary structure nature.

The dark recovery rate of the LOVcore+Jα$_5$ construct (Fig. 1c and Fig. S1d) is much lower than all the previously reported rates for other LOV domains.[16] Additionally, we report here the highest E_{act} of the dark recovery rate for a LOV domain (126 kJ/mol) (Fig. S1e). Compared to the isolated YtvA LOV core (residues 26–127), the half-life obtained here for the *Brucella* LOV domain at 25 °C is 40 times larger (1860 *versus* 45 min). The difference is due to a twice larger E_{act}, while the pre-exponential factor is 8 orders of magnitude larger.[40] Thus, the high E_{act} of the *Brucella* LOV domain seems to be the basis for the long lifetime of the covalent photoadduct. Still, there is no obvious correlation in the amino acid sequence that can easily account for this large E_{act}.

The stability of the *Brucella* LOV domain depends on the light conditions. The dark state is more stable, showing minor changes in the NMR spectra after several days at 35 °C; while in the lit state, evidences of proteolysis are seen after 5 days. The instability of the lit state has already been reported for other LOV domains.[7,41] Nevertheless, the lit conformation of the *Brucella* LOV domain is stable enough to allow for the almost complete chemical shift assignment of the backbone nuclei.

The crystal structure as well as NMR spectroscopy demonstrated the presence of a five-residue-long helical region C-terminal to the Iβ-strand (the Jα-helix), which points towards the solvent. The same extended orientation of the Jα-helix has been reported in the crystal structure of the LOV domain of Ytva.[11] Small-angle X-ray scattering experiments indicate that the LOV domain of *C. crescentus* LOV-HK adopts the same orientation.[16] The presence of a coiled-coil signature in the Jα-helix sequence of the *Brucella* LOV domain suggests that, as observed for the LOV domain of Ytva, the Jα-helix should participate in the dimerization of the protein. A number of PAS-HK proteins present a coiled-coil helix between the sensor and the output domains, which is proposed to play a central role in the mechanism of signal transmission *via* rotation.[31] In *Brucella* LOV-HK, the predicted coiled-coil helix is located between the LOV and PAS domains. The presence of a coiled-coil dimerization motif in the *Brucella* LOV-HK and its role in the signal propagation mechanism should be experimentally addressed.

The *Brucella* LOV domain is an HT dimer both in the crystal (Fig. 3a) and in solution (Fig. 5). The dimerization interface comprises the hydrophobic β-scaffold. From the comparison with other LOV domains, we have noticed that the β-sheet is always buried, interacting with other monomers or with other parts of the protein (Fig. 3b and c). In all LOV domains, the β-sheet is mainly hydrophobic. The hydrophobicity of the β-sheet provides the LOV domain with a sticky surface that accommodates other LOV domain as in YtvA,[11] the N-terminal helix N-cap in Vivid,[8] the Jα-helix in AsLOV2,[32] and the DNA-binding domain in EL222.[9] The tendency to dimerize through the β-scaffold and its role in the signal propagation have been reported not only for LOV domains but also for a large number of PAS domains, indicating that these are general features of the PAS superfamily.[42] The PAS-A domain of KinA from *B. subtilis* clearly illustrates this common mechanism.[43] The PAS-A domain is a dimer in solution. Two different dimerization arrangements were found in the crystal structure comprising the β-scaffold. This interacting surface presents conformational instability since, like for the *Brucella* LOV domain, the cross peaks corresponding to the β-scaffold were not observed in the ^{15}N–^{1}H HSQC spectra. The cross peaks only appeared after destabilizing the dimerization surface by point mutations. Furthermore, these mutations showed that the β-scaffold is essential in the regulation of the kinase activity, with implications in the bacterial physiology.

Taking into account that all histidine kinases described to date are parallel dimers,[44] an HT dimerization is not likely to occur in the full-length

protein. The HT arrangement of the *Brucella* LOV domain dimer is conformationally unstable, and this instability could be attributed to its artificial nature (Fig. 5b and Fig. S6). This dimer is probably formed due to the large hydrophobic area of the β-scaffold that cannot be exposed to the solvent. In the full-length protein, the hydrophobic β-sheet probably interacts either with the PAS domain or the Jα-helix or, alternatively, with the LOV domain of the second monomer in an HH orientation. If the latter case were true, our results would suggest that the LOVcore+Jα_5 construct *per se* might not contribute enough to maintain the dimer in its parallel arrangement.

Having the protein assigned in both states allowed us to obtain a good estimation of the chemical shift perturbations induced by light. A global comparison of the chemical shift perturbation indicates that in our case, the chemical shift differences are intermediate between those ones observed for AsLOV2[7] and EL222.[9] In AsLOV2, a disruption of the interaction between the Jα-helix and the β-sheet surface of the LOV2 is observed upon illumination, with the concomitant unfolding of the helix. In EL222, blue light breaks the interaction between the LOV domain and the DNA-binding domain that occurs through the β-sheet scaffold. Upon illumination, the *Brucella* LOV domain undergoes local changes involving the αE-helix, which contains the active cysteine, the αD-helix, and the Gβ-, Hβ-, and Iβ-strands. The same regions were reported to suffer light-induced conformational changes in the EL222 and AsLOV2 domains. Thus, most of the conformational changes induced by light are concentrated in the β-scaffold. There is increasing experimental evidence that the β-sheet is a key transducer element of signal propagation.[17,27] One side of the β-scaffold is part of the pocket in which the FMN molecule reacts to blue light and the other side interacts with other parts of the protein. Our results point to the β-scaffold as a key transducer element, validating a conserved structural basis for light-to-signal transduction in LOV proteins, where light-induced conformational changes trigger activation *via* the β-scaffold. The interacting surface and the signal propagation downstream the β-surface is different in each protein. Finding out the interacting partner surface of the LOV domain β-scaffold in *Brucella* LOV-HK may reveal further details of the molecular mechanisms of light activation.

Materials and Methods

Cloning and purification

The DNA fragments encoding residues 28–154 (LOVcore+Jα_{20}) and 28–139 (LOVcore+Jα_5) of LOV-HK were amplified from *B. abortus* genomic DNA *via* PCR and cloned into the pET24d vector (Novagen, Madison, WI) using NheI and XhoI restriction sites. BL21 *Escherichia coli* cells were transformed with the recombinant plasmids and grown under dark conditions for 3 h at 37 °C followed by 16 h at 28 °C from an overnight preculture. Autoinducing medium[45] was used for the preparations for crystallization, absorption spectra measurements, and limited proteolysis assays. M9 minimal medium containing $^{15}NH_4Cl$ as the sole nitrogen source and $^{15}NH_4Cl/^{13}C_6$ glucose as the sole nitrogen and carbon sources was used for the NMR studies. In the latter preparations, 0.25 mM IPTG was added for induction. Cell lysis was carried out by sonication in a buffer containing 20 mM Tris–HCl, pH 8.0, 500 mM NaCl, 20 mM imidazole, 0.1% v/v Triton X-100, and 1 mM DTT. The proteins were purified *via* Ni^{2+}-affinity chromatography from the soluble fractions, except for the NMR studies, where it was obtained from the insoluble fractions due to the lower amounts in the supernatants. Inclusion bodies were solubilized in 6 M urea, and Ni^{2+}-affinity chromatography was performed under denaturing conditions. The eluates were incubated with an excess of FMN overnight at 18 °C and dialyzed against 20 mM Tris–HCl, 50 mM NaCl, 0.5 mM DTT, and 0.5 mM ethylenediaminetetraacetic acid (EDTA) for crystallization, and 50 mM sodium phosphate, pH 7.0, 100 mM NaCl, 0.5 mM DTT, and 0.5 mM EDTA for the NMR studies. The proteins were further purified with a Superdex 75 column (GE Healthcare) using the same buffers, concentrated by centrifugation, and stored at −80 °C.

Dark-state recovery rate measurements

Absorption and lit minus dark spectra were collected every 30 min for 12 h on a Hewlett Packard 8452A Diode Array Spectrometer as described previously.[6] The optical path length was 1 cm. The light pulse was provided by a white light camera strobe flash. Temperature was not controlled but measured to be 20 ± 2 °C. The protein concentration was 1 mg/ml.

NMR dark recovery rate measurements were performed by following the low-field FMN N(3)H signal of the flavin in the ^1H spectrum (Fig. S1a), which resonates in a clean region at 11.8 and 12.5 ppm in the lit and dark states of the protein, respectively (Fig. S1a and b). Further details are presented below.

Crystallization and data collection

The LOVcore+Jα_5 construct (10–15 mg/ml) was crystallized under dark conditions at 19 °C by means of the hanging drop vapor diffusion method in 25% (w/v) polyethylene glycol monomethyl ether 2000 and 100 mM Tris–HCl, pH 7.5. Diamond-shaped crystals of about 0.2 mm × 0.2 mm × 0.2 mm appeared within a week. Crystals were then transferred to a cryoprotectant solution consisting of mother liquor added with 20% (v/v) glycerol, mounted in Hampton Research cryoloops (Aliso Viejo, CA), and flash cooled in liquid nitrogen. X-ray diffraction data were collected at 100 K at the Institut Pasteur Montevideo, Uruguay, on a MicroMax-007 HF rotating anode diffractometer (Rigaku, The Woodlands,

TX) equipped with a copper rotating anode and a MAR345 image plate detector (Marresearch, Norderstedt, Germany). Data processing was performed with XDS.[46] Data collection and processing statistics are shown in Table 1.

Structure determination and refinement

The LOV domain crystal structure was solved by molecular replacement using AMoRe[47] as implemented in the CCP4 package.[48] The crystal structure of LOV2 from oat Phototropin1 (PDB code 2V0U) was used as search model. Two copies of the monomer were unambiguously found in the asymmetric unit after the rotation and translation steps performed between 15 and 4 Å resolution. The oriented coordinates were then subjected to several cycles of positional and *B*-factor refinement with Refmac5.[49] Between these individual cycles, model building was performed with Coot.[50] Both monomers were refined independently without the application of non-crystallographic symmetry. At the last stages of the process, solvent and ligand atoms were added to the model. The final refinement converged to $R=0.195$ and $R_{free}=0.222$. The structure was validated with PROCHECK,[51] Coot, and the Validation Server from the PDB.

Graphical representation of the models

Figures were prepared with PyMOL (DeLano Scientific).[52]

Structure analysis and comparison

For the buried solvent-accessible area calculations, the PISA web server was used.[53] rmsd calculations were performed using the program DaliLite. The dimerization interface was analyzed using the PISA web server and Contact under the CCP4 package.

NMR spectroscopy samples and conditions

Final samples for NMR experiments contained ~1 mM ^{15}N or $^{15}N/^{13}C$-labeled protein, 100 mM NaCl, 20 mM sodium phosphate, pH 7.0, 0.5 mM DTT, and 0.5 mM EDTA, in a mixture of 90% H_2O/10% D_2O. The NMR experiments were performed at 308 K on a Bruker 600-MHz Avance III spectrometer equipped with a 5-mm triple-resonance cryoprobe incorporating shielded *z*-axis gradient coils. The NMR data were processed on Silicon Graphics workstations using NMRPipe[54] and analyzed using NMRView.[55]

We controlled the dark- and lit-state homogeneity of the samples by following the N(3)H signal of the flavin in the ^1H spectrum (Fig. S1). As shown in Fig. S2, this hydrogen group binds to the carbonyl group of Asn101, protecting the N(3)H from the solvent exchange. In the lit state, the N(3)H proton signal appears at 12.5 ppm, and in the dark state, it appears at 11.9 ppm. These signals are in slow exchange in the experimental conditions. To perform the lit-state spectra, we illuminated the sample with a constant light source during acquisition using a system consisting of a high-power (3 W) blue light LED (maximum, 467 nm) coupled to a 1-mm-core-diameter fiber optic (Newport). One end of the fiber optic was coupled to the LED and the other end was held inside the NMR tube immersed into the sample. The fluency measured at the tip of the fiber optic was approximately 2500 μmol/m^2/s (Quantum Meter, Apogee Instruments).

Chemical shift assignment

The following standard set of triple-resonance spectra were acquired in H_2O: HNCO, HNCA, HN(CO)CA, HN(CA)CO, HACACO, CBCA(CO)NH, and HAHB(CO)NH in order to assign the backbone of the protein. Also, ^{15}N-NOESY and ^{15}N-TOCSY (total correlated spectroscopy) (mixing times of 100 and 30 ms, respectively) and constant-time $^1H^{-13}C$ HSQC experiments were performed. Mainly, the same experiments were performed to assign the backbone resonances of the lit state of the *Brucella* LOV domain. However, due to the sample instability in the lit conditions, we used several fresh samples to record the whole set of NMR spectra.

Backbone ϕ and φ dihedral angles were predicted from backbone chemical shifts of dark and lit states using the program TALOS+.[34]

Chemical shift perturbation analysis

For the analysis, in the cases in which assignment was made in both lit and dark states, we used the average chemical shift perturbation, $\Delta\delta_{av}=[(\Delta\delta^2_{NH}+\Delta\delta^2_{N}/25)/2]^{1/2}$ (ppm).[38] In the cases where it was not possible to identify the position of the cross peaks of the lit state (residues Cys69, Arg70, Phe71, Leu113, His114, Ile115, and Ser116), the minimum chemical shift difference method[39] was applied ($\Delta\delta_{min}=[(\Delta\delta^2_{NH}+0.17*\Delta\delta^2_{N}+0.39*\Delta\delta^2_{CO})]^{1/2}$).

Diffusion measurements of the dark state

The pulsed field gradient NMR self-diffusion measurements were performed using the PGSLED sequence.[56] Dioxane (10 μL, 2% in D_2O) was added to the sample as internal standard.[35] The length of all pulses and delays in the sequence was held constant and 19 spectra were acquired with the strength of the diffusion gradient varying between 5% and 95% of its maximum value. The pulse gradient width was 4 ms, and the length of the diffusion delay was calibrated for the sample in order to give a total decay of 85–90% for the protein and dioxane signals. A T_2 filter was used to selectively observe the dioxane signal without interference of the protein. The dioxane NMR spectra were acquired with 16K complex points, and the protein NMR spectra were acquired with 4K complex points. For the protein, a number of high-field methyl and low-field amide groups were selected and integrated. The hydrodynamic radius was determined fitting the intensities of the corresponding protein and dioxane signals to an exponential function of the square of the gradient strength:

$$s(g) = A\exp\left[dg^2(\Delta - \delta/3)\right]$$

where, $s(g)$ is the measured peak intensity, Δ is the diffusion delay experimentally determined for each molecule, δ is the duration of gradient (4 ms), g is the fraction of the maximum gradient strength used in each experiment (from 0.05 to 0.95), and d is a constant proportional to the translational diffusion coefficient D. In accordance with the Stokes–Einstein equation, D is inversely proportional to the hydrodynamic radius. Therefore, from the relationship between the d values obtained for dioxane and protein, it is possible to calculate the hydrodynamic protein radius: $R_h^{prot} = R_h^{diox}$ (d_{diox}/d_{prot}), $R_h^{diox} = 2.12$ Å. The KaleidaGraph 4.0 package was used to perform the fittings. The measurements were repeated three times to ensure reproducibility.

^{15}N relaxation measurements and backbone dynamics of the dark state

Measurements of ^{15}N T_1, T_2, and ^{1}H–^{15}N NOE were performed at the 60.83-MHz ^{15}N frequency using standard pulse schemes in an interleaved manner. Relaxation delays of 8, 17, 34, 51, 68, 85, 102, and 119 ms were employed for T_2, and delays of 16, 282, 563, 857, 1124, 1685, and 2106 ms were employed for T_1. Data were fitted using the Rate Analysis routine of NMRView.[55] The heteronuclear NOE values were determined by the ratio of peak volumes of spectra recorded with and without ^{1}H saturation, employing a net relaxation delay of 4 s for each scan in both experiments. Each measurement was repeated twice to ensure reproducibility. Typically, errors were about 2% for T_1 and T_2, and 4% for ^{1}H–^{15}N NOE measurements. The rotational correlation time was calculated based on T_1/T_2 values as previously obtained.[57]

Dynamic parameter calculations

The HYDRONMR software[36] was used in order to predict the hydrodynamic radii and the rotational diffusion constants of the LOV domain monomer and of the HT and HH dimers. For the monomer and the HT dimer, the coordinates of the crystal structure were used in the calculations. The coordinates of the HH dimer were generated by rotating and displacing one of the monomers in the crystal structure in search of maximizing the interaction surface between monomers. The T_1/T_2 values for the same molecules at 600 MHz were calculated with the same software. We found that the mean calculated values are slightly smaller than the experimental ones. The differences are attributed to the fact that the coordinates do not include the flexible C-terminal cloning artifact. Since the goal was to compare the dispersion and the relative variation per residue, we decided to adjust the viscosity coefficient values in the calculations in order to match the mean experimental T_1/T_2 ratio. The viscosity coefficient values obtained were 1.18 and 1.28 (relative to pure water at 35 °C) for the HT and HH dimers, respectively, which are reasonable for a highly concentrated protein solution. In fact, no signs of protein aggregation were observed since the R_h did not vary over the protein concentration.

Accession numbers

Atomic coordinates and structure factors of the LOV domain of LOV-HK from *B. abortus* structure in its dark conformation have been deposited at the PDB under the accession code 3T50.

Acknowledgements

We are grateful to Dr. Leonardo Alonso (Fundación Instituto Leloir) for mass spectrometry analysis and to Dr. Alejandro Buschiazzo (Institut Pasteur Protein Crystallography Facility) and Dr. William Shephard (Synchrotron SOLEIL) for their help in data collection and processing. This work was supported by the Consejo Nacional de Investigaciones Científicas y Técnicas, the Agencia Nacional de Promoción Científica y Tecnológica, and the Howard Hughes Medical Institute R.A.B. is supported by NSF-0843662.

Supplementary Data

Supplementary data associated with this article can be found, in the online version, at doi:10.1016/j.jmb.2012.04.006

References

1. Taylor, B. L. & Zhulin, I. B. (1999). PAS domains: internal sensors of oxygen, redox potential, and light. *Microbiol. Mol. Biol. Rev.* **63**, 479–506.
2. Liscum, E. & Briggs, W. R. (1995). Mutations in the NPH1 locus of *Arabidopsis* disrupt the perception of phototropic stimuli. *Plant Cell*, **7**, 473–485.
3. Imaizumi, T., Tran, H. G., Swartz, T. E., Briggs, W. R. & Kay, S. A. (2003). FKF1 is essential for photoperiodic-specific light signalling in *Arabidopsis*. *Nature*, **426**, 302–306.
4. Avila-Perez, M., Hellingwerf, K. J. & Kort, R. (2006). Blue light activates the sigmaB-dependent stress response of *Bacillus subtilis* via YtvA. *J. Bacteriol.* **188**, 6411–6414.
5. Salomon, M., Christie, J. M., Knieb, E., Lempert, U. & Briggs, W. R. (2000). Photochemical and mutational analysis of the FMN-binding domains of the plant blue light receptor, phototropin. *Biochemistry*, **39**, 9401–9410.
6. Swartz, T. E., Corchnoy, S. B., Christie, J. M., Lewis, J. W., Szundi, I., Briggs, W. R. & Bogomolni, R. A. (2001). The photocycle of a flavin-binding domain of the blue light photoreceptor phototropin. *J. Biol. Chem.* **276**, 36493–36500.
7. Harper, S. M., Neil, L. C. & Gardner, K. H. (2003). Structural basis of a phototropin light switch. *Science*, **301**, 1541–1544.
8. Zoltowski, B. D., Schwerdtfeger, C., Widom, J., Loros, J. J., Bilwes, A. M., Dunlap, J. C. & Crane, B. R. (2007). Conformational switching in the fungal light sensor Vivid. *Science*, **316**, 1054–1057.
9. Nash, A. I., McNulty, R., Shillito, M. E., Swartz, T. E., Bogomolni, R. A., Luecke, H. & Gardner, K. H. (2011).

Structural basis of photosensitivity in a bacterial light–oxygen–voltage/helix–turn–helix (LOV–HTH) DNA-binding protein. *Proc. Natl Acad. Sci. USA*, **108**, 9449–9454.
10. Jurk, M., Dorn, M. & Schmieder, P. (2011). Blue flickers of hope: secondary structure, dynamics, and putative dimerization interface of the blue-light receptor YtvA from *Bacillus subtilis*. *Biochemistry*, **50**, 8163–8171.
11. Moglich, A. & Moffat, K. (2007). Structural basis for light-dependent signaling in the dimeric LOV domain of the photosensor YtvA. *J. Mol. Biol.* **373**, 112–126.
12. Buttani, V., Gartner, W. & Losi, A. (2007). NTP-binding properties of the blue-light receptor YtvA and effects of the E105L mutation. *Eur. Biophys. J.* **36**, 831–839.
13. Harper, S. M., Christie, J. M. & Gardner, K. H. (2004). Disruption of the LOV–Jalpha helix interaction activates phototropin kinase activity. *Biochemistry*, **43**, 16184–16192.
14. Losi, A., Ghiraldelli, E., Jansen, S. & Gartner, W. (2005). Mutational effects on protein structural changes and interdomain interactions in the blue-light sensing LOV protein YtvA. *Photochem. Photobiol.* **81**, 1145–1152.
15. Tang, Y., Cao, Z., Livoti, E., Krauss, U., Jaeger, K. E., Gartner, W. & Losi, A. (2010). Interdomain signalling in the blue-light sensing and GTP-binding protein YtvA: a mutagenesis study uncovering the importance of specific protein sites. *Photochem. Photobiol. Sci.* **9**, 47–56.
16. Purcell, E. B., McDonald, C. A., Palfey, B. A. & Crosson, S. (2010). An analysis of the solution structure and signaling mechanism of LovK, a sensor histidine kinase integrating light and redox signals. *Biochemistry*, **49**, 6761–6770.
17. Losi, A. & Gartner, W. (2011). Old chromophores, new photoactivation paradigms, trendy applications: flavins in blue light-sensing photoreceptors. *Photochem. Photobiol.* **87**, 491–510.
18. Crosson, S. & Moffat, K. (2001). Structure of a flavin-binding plant photoreceptor domain: insights into light-mediated signal transduction. *Proc. Natl Acad. Sci. USA*, **98**, 2995–3000.
19. Fedorov, R., Schlichting, I., Hartmann, E., Domratcheva, T., Fuhrmann, M. & Hegemann, P. (2003). Crystal structures and molecular mechanism of a light-induced signaling switch: the Phot-LOV1 domain from *Chlamydomonas reinhardtii*. *Biophys. J.* **84**, 2474–2482.
20. Nakasako, M., Zikihara, K., Matsuoka, D., Katsura, H. & Tokutomi, S. (2008). Structural basis of the LOV1 dimerization of *Arabidopsis* phototropins 1 and 2. *J. Mol. Biol.* **381**, 718–733.
21. Jurk, M., Dorn, M., Kikhney, A., Svergun, D., Gartner, W. & Schmieder, P. (2010). The switch that does not flip: the blue-light receptor YtvA from *Bacillus subtilis* adopts an elongated dimer conformation independent of the activation state as revealed by a combined AUC and SAXS study. *J. Mol. Biol.* **403**, 78–87.
22. Briggs, W. R. (2007). The LOV domain: a chromophore module servicing multiple photoreceptors. *J. Biomed. Sci.* **14**, 499–504.
23. Crosson, S. & Moffat, K. (2002). Photoexcited structure of a plant photoreceptor domain reveals a light-driven molecular switch. *Plant Cell*, **14**, 1067–1075.
24. Crosson, S., Rajagopal, S. & Moffat, K. (2003). The LOV domain family: photoresponsive signaling modules coupled to diverse output domains. *Biochemistry*, **42**, 2–10.
25. Losi, A. (2004). The bacterial counterparts of plant phototropins. *Photochem. Photobiol. Sci.* **3**, 566–574.
26. Losi, A., Polverini, E., Quest, B. & Gartner, W. (2002). First evidence for phototropin-related blue-light receptors in prokaryotes. *Biophys. J.* **82**, 2627–2634.
27. Herrou, J. & Crosson, S. (2011). Function, structure and mechanism of bacterial photosensory LOV proteins. *Nat. Rev. Microbiol.* **9**, 713–723.
28. Swartz, T. E., Tseng, T. S., Frederickson, M. A., Paris, G., Comerci, D. J., Rajashekara, G. *et al.* (2007). Blue-light-activated histidine kinases: two-component sensors in bacteria. *Science*, **317**, 1090–1093.
29. Lupas, A., Van Dyke, M. & Stock, J. (1991). Predicting coiled coils from protein sequences. *Science*, **252**, 1162–1164.
30. McDonnell, A. V., Jiang, T., Keating, A. E. & Berger, B. (2006). Paircoil2: improved prediction of coiled coils from sequence. *Bioinformatics*, **22**, 356–358.
31. Moglich, A., Ayers, R. A. & Moffat, K. (2009). Design and signaling mechanism of light-regulated histidine kinases. *J. Mol. Biol.* **385**, 1433–1444.
32. Halavaty, A. S. & Moffat, K. (2007). N- and C-terminal flanking regions modulate light-induced signal transduction in the LOV2 domain of the blue light sensor phototropin 1 from *Avena sativa*. *Biochemistry*, **46**, 14001–14009.
33. Alexandre, M. T., Arents, J. C., van Grondelle, R., Hellingwerf, K. J. & Kennis, J. T. (2007). A base-catalyzed mechanism for dark state recovery in the *Avena sativa* phototropin-1 LOV2 domain. *Biochemistry*, **46**, 3129–3137.
34. Shen, Y., Delaglio, F., Cornilescu, G. & Bax, A. (2009). TALOS+: a hybrid method for predicting protein backbone torsion angles from NMR chemical shifts. *J. Biomol. NMR*, **44**, 213–223.
35. Wilkins, D. K., Grimshaw, S. B., Receveur, V., Dobson, C. M., Jones, J. A. & Smith, L. J. (1999). Hydrodynamic radii of native and denatured proteins measured by pulse field gradient NMR techniques. *Biochemistry*, **38**, 16424–16431.
36. Garcia de la Torre, J., Huertas, M. L. & Carrasco, B. (2000). HYDRONMR: prediction of NMR relaxation of globular proteins from atomic-level structures and hydrodynamic calculations. *J. Magn. Reson.* **147**, 138–146.
37. Ryabov, Y., Schwieters, C. D. & Clore, G. M. (2011). Impact of ^{15}N R2/R1 relaxation restraints on molecular size, shape, and bond vector orientation for NMR protein structure determination with sparse distance restraints. *J. Am. Chem. Soc.* **133**, 6154–6157.
38. Grzesiek, S., Bax, A., Clore, G. M., Gronenborn, A. M., Hu, J. S., Kaufman, J. *et al.* (1996). The solution structure of HIV-1 Nef reveals an unexpected fold and permits delineation of the binding surface for the SH3 domain of Hck tyrosine protein kinase. *Nat. Struct. Biol.* **3**, 340–345.
39. Farmer, B. T., II, Constantine, K. L., Goldfarb, V., Friedrichs, M. S., Wittekind, M., Yanchunas, J., Jr. *et al.*

(1996). Localizing the $NADP^+$ binding site on the MurB enzyme by NMR. *Nat. Struct. Biol.* **3**, 995–997.
40. Losi, A., Quest, B. & Gartner, W. (2003). Listening to the blue: the time-resolved thermodynamics of the bacterial blue-light receptor YtvA and its isolated LOV domain. *Photochem. Photobiol. Sci.* **2**, 759–766.
41. Yao, X., Rosen, M. K. & Gardner, K. H. (2008). Estimation of the available free energy in a LOV2–J alpha photoswitch. *Nat. Chem. Biol.* **4**, 491–497.
42. Moglich, A., Ayers, R. A. & Moffat, K. (2009). Structure and signaling mechanism of Per-ARNT-Sim domains. *Structure*, **17**, 1282–1294.
43. Lee, J., Tomchick, D. R., Brautigam, C. A., Machius, M., Kort, R., Hellingwerf, K. J. & Gardner, K. H. (2008). Changes at the KinA PAS-A dimerization interface influence histidine kinase function. *Biochemistry*, **47**, 4051–4064.
44. Casino, P., Rubio, V. & Marina, A. (2010). The mechanism of signal transduction by two-component systems. *Curr. Opin. Struct. Biol.* **20**, 763–771.
45. Studier, F. W. (2005). Protein production by auto-induction in high density shaking cultures. *Protein Expr. Purif.* **41**, 207–234.
46. Kabsch, W. (2010). XDS. *Acta Crystallogr., Sect. D: Biol. Crystallogr.* **66**, 125–132.
47. Navaza, J. (1994). AMoRe: an automated package for molecular replacement. *Acta Crystallogr., Sect. A*, **50**, 157–163.
48. Collaborative Computation Project, No. 4 (1994). The CCP4 suite: programs for protein crystallography. *Acta Crystallogr., Sect. D: Biol. Crystallogr.* **50**, 760–763.
49. Murshudov, G. N., Vagin, A. A. & Dodson, E. J. (1997). Refinement of macromolecular structures by the maximum-likelihood method. *Acta Crystallogr., Sect. D: Biol. Crystallogr.* **53**, 240–255.
50. Emsley, P. & Cowtan, K. (2004). Coot: model-building tools for molecular graphics. *Acta Crystallogr., Sect. D: Biol. Crystallogr.* **60**, 2126–2132.
51. Laskowski, R. A., Moss, D. S. & Thornton, J. M. (1993). Main-chain bond lengths and bond angles in protein structures. *J. Mol. Biol.* **231**, 1049–1067.
52. DeLano, W. L. (2002). *The PyMOL Molecular Graphics System.*
53. Krissinel, E. & Henrick, K. (2007). Inference of macromolecular assemblies from crystalline state. *J. Mol. Biol.* **372**, 774–797.
54. Delaglio, F., Grzesiek, S., Vuister, G. W., Zhu, G., Pfeifer, J. & Bax, A. (1995). NMRPipe: a multidimensional spectral processing system based on UNIX pipes. *J. Biomol. NMR*, **6**, 277–293.
55. Johnson, B. A. (2004). Using NMRView to visualize and analyze the NMR spectra of macromolecules. *Methods Mol. Biol.* **278**, 313–352.
56. Jones, J. A., Wilkins, D. K., Smith, L. J. & Dobson, C. M. (1997). Characterization of protein unfolding by NMR diffusion measurements. *J. Biomol. NMR*, **10**, 199–203.
57. Viles, J. H., Donne, D., Kroon, G., Prusiner, S. B., Cohen, F. E., Dyson, H. J. & Wright, P. E. (2001). Local structural plasticity of the prion protein. Analysis of NMR relaxation dynamics. *Biochemistry*, **40**, 2743–2753.